Report

AMESP - Phase 2 WP3

NHL STENDEN
hogeschool

Contents

1 WP3 Overview

1.1 Objectives

As stated on the proposal, we have two main goals in the WP3:

1. Investigate methods to identify the electrospray mode during operation by reading current values

2. Investigate methods to perform corrective actions to restore the electrospray operation by sending commands to the pump and/or power supply

We have explored two approaches that could achieve these goals, and they are detailed on Sections 2 and 3. For each approach, we discuss how they can be implemented in the system developed by Gilbert, their advantadges and disadvantages, and how well they perform in achieve the above goals.

Section 4 shows some results obtained during the control investigations that were not directly used to achieve the goals of this Work Package, but we believe they could still prove useful to Gilbert and provide inputs to how the multinozzle prototype operates.

1.2 Timeline of Executed Tasks

Figure 1 shows a timeline of executed tasks for Work Package 3.

Tasks	July				August				September				October				November				December			
	1	2	3	4	1	2	3	4	1	2	3	4	1	2	3	4	1	2	3	4	1	2	3	4
PID Controller Investigations	▓	▓	▓	▓	▓	▓																		
Time Response Analysis					▓	▓																		
Pump Disturbances									▓	▓	▓													
3 currents measurements										▓	▓	▓	▓											
Reproducing Single Nozzle													▓	▓										
Crown Influences Investigations													▓	▓	▓									
Classifying the spray mode														▓	▓	▓								
Optimizing the Classification																	▓	▓	▓					
POC Real-Time EHDA Classification																			▓	▓	▓	▓	▓	
POC Real-Time EHDA Control																					▓	▓		

Figure 1. Timeline of executed tasks.

The tasks on Figure 1 relate directly to the sections of this report in the table of contents. The gap between August and September corresponds to the holiday period of several members of the project. Tasks executed of other Work Packages are not included in the timeline.

1.3 Conventions

Throughout this report, we'll refer multiple times to physical variables of the system. Figure 2 shows the variable conventions we'll use in this text.
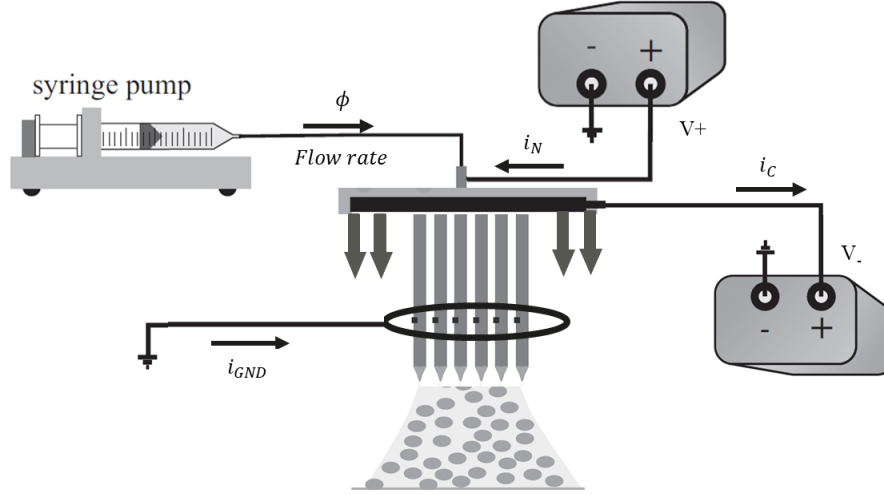
Figure 2. Variable conventions and nomenclature. Source: adapted from Verdoold et al. (2013).

As shown in Figure 2, we have

- i_N: current flowing from the positive high voltage source to the nozzles

- i_C: current flowing from the crown to the negative high voltage source

- i_{GND}: current flowing from the ground to the ring

- ϕ: flow rate of the syringe pump

- V_+: voltage of the positive high voltage source

- V_-: voltage of the negative high voltage source

The direction of the currents was chosen as shown in Figure 2 to ensure they are always positve in the measurements, faciliting the analysis.

2 First Approach: PID Controller

2.1 Time Response Analysis

2.2 Pump Disturbances

3 Second Approach: Current-based Classification and Control

Once identified the issues with the first approach, we attempted to design a controller based on the classification suggested by Verdoold et al. (2013).

The strategy adopted will be to first classify the electrospray mode by looking a current values on the system, and then experimentally design a controller that can move from an intermittent to a cone-jet spray mode.

However, Verdoold's method was designed for the single nozzle, and it is not clear if we can extend his classification to a multinozzle configuration. Therefore, part of this work includes an attempt to extend his classification to the system developed by Gilbert.

3.1 Measuring the currents by spray mode

The first test done was to measure the current on all three lines of the sprayhead and verify if we see a pattern in the shape of current that can be used to classify the spray mode. Figure 3 shows the setup used for this test. V_- was fixed on $V_- = -4.5kV$.

Using three oscilloscopes, all three currents were sampled at 5 kHz, collecting 20.000 samples of each (totalling a 4 seconds time window). Notice that, although the oscilloscope has multiple channels, we cannot use the same oscilloscope as the channels are interconnected internally: the high voltage differences would damage the instrument. Therefore, we use one oscilloscope for each line.

Figure 4 and Figure 5 show the waveforms obtained for $\phi = 20\,\mathrm{mL/h}; \phi = 30\,\mathrm{mL/h}; \phi = 50\,\mathrm{mL/h}$ for two different time windows: 50ms and 500ms.

As we can see in Figure 4 and Figure 5, we don't see a clear distinction in the shape of the current by different spray modes, in both time windows. The sharp peaks we see on the waveforms are most likely caused by a high-frequency noise in signal, especially since we use banana adapters for the oscilloscope in this test, instead of coaxial cables, which pick up less noise.

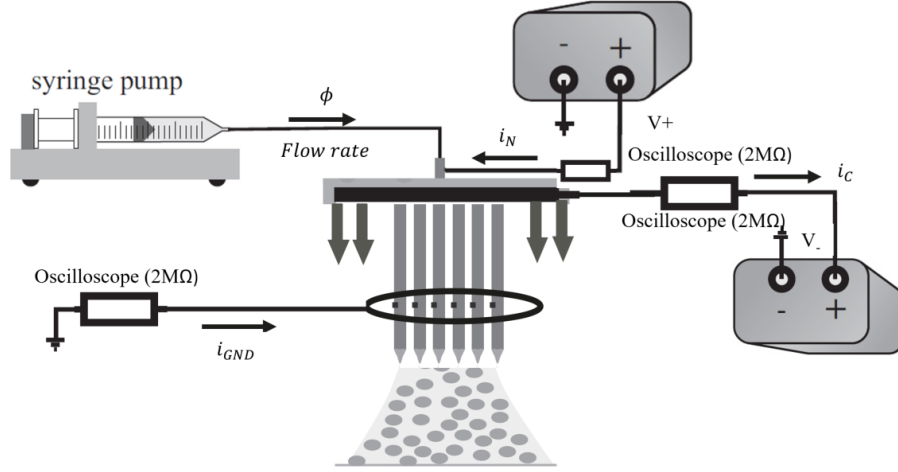Attempting to see a distinction on Figure 5 via the standard deviation also fails, as

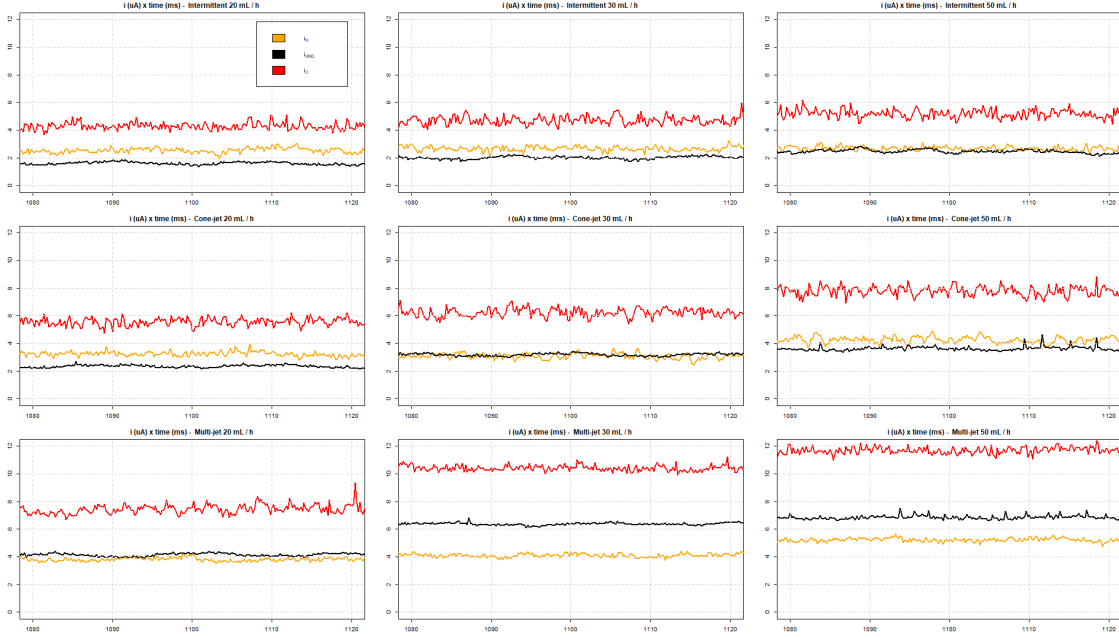**Figure 3.** Setup to measure all three currents on the sprayhead. Source: adapted from Verdoold et al. (2013).

Figure 4. i_N, i_{GND} and i_C over time by different spray modes - 50 ms time window.

shown on Figure 6.

Without a clear distinction in the current waveforms it would not possible to continue with this approach. Therefore, we need to first understand why we are not seing distinctions in the shape of the current, particularly between the intermittent and cone-jet spray modes, as it is clear in the literature that there should be a difference.

To do this, we'll begin by attempting to reproduce Verdoold et al. (2013)'s results, with the goal of isolating if the problem is our measurement strategy or if it is something related to the sprayhead itself.
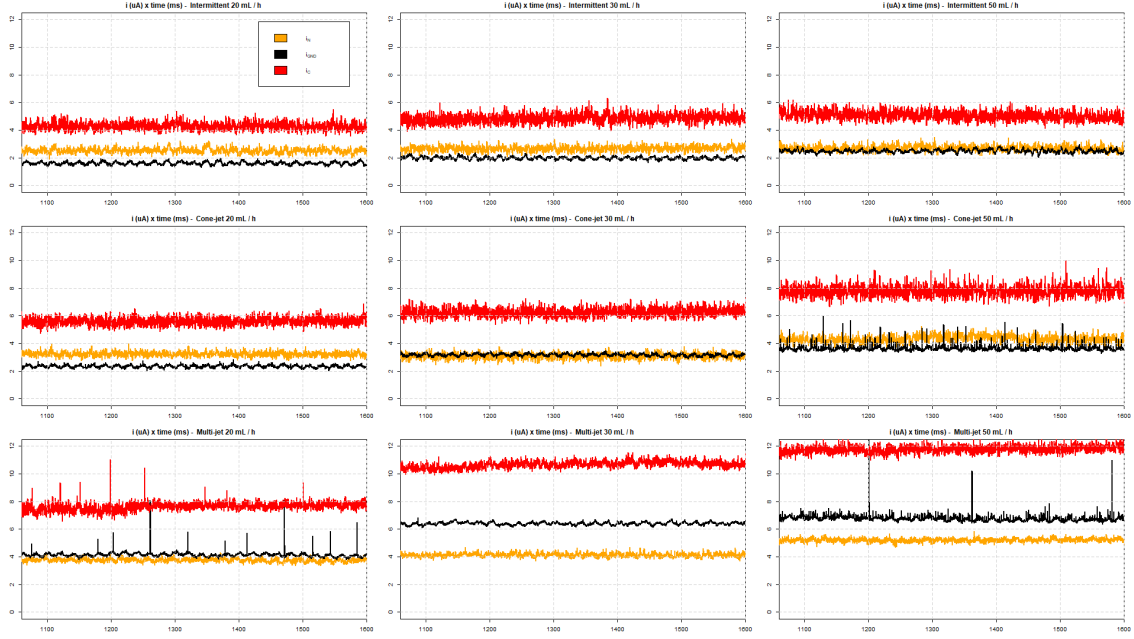
5

Figure 5. i_N, i_{GND} and i_C over time by different spray modes - 500 ms time window.
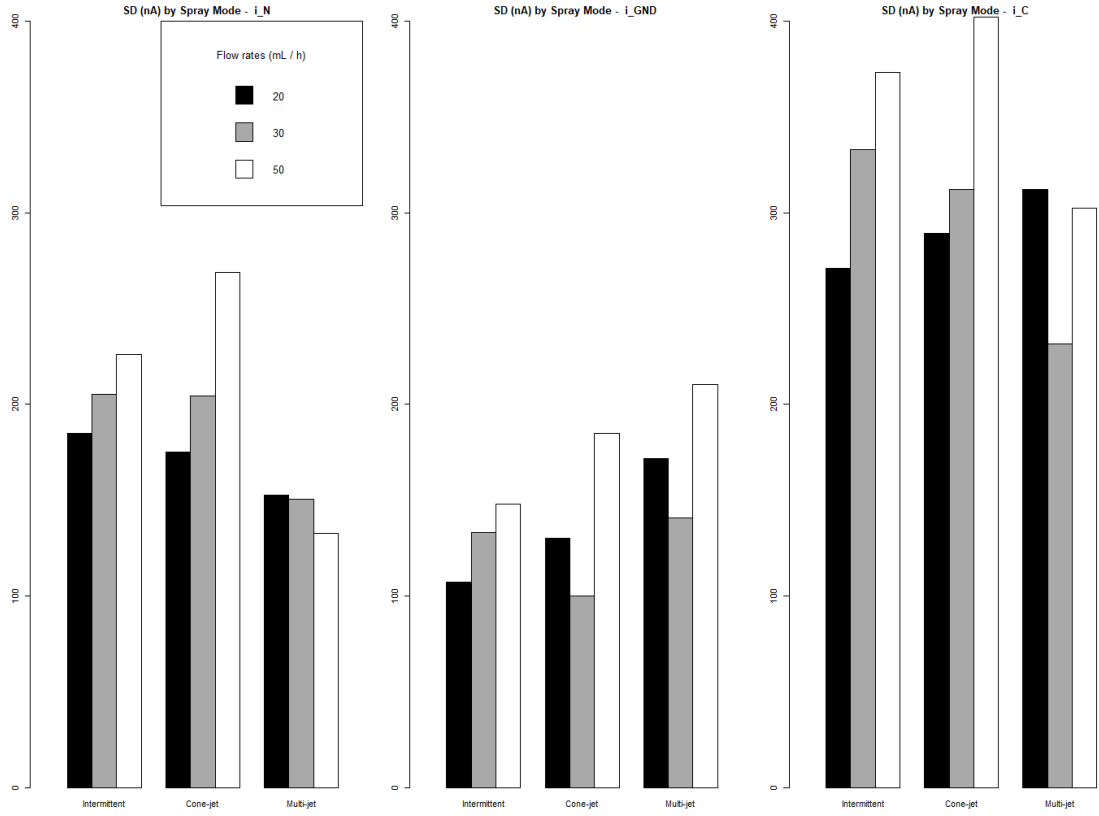

Figure 6. Standard deviation on Figure 5 of i_N, i_{GND} and i_C by spray mode.

3.2   Reproducing Results from Verdoold et al. (2013)

Figure 7 shows the setup used to reproduce Verdoold et al. (2013)'s approach. We used a sampling frequency of 5 kHz and $\phi = 1\,\mathrm{mL/h}$.
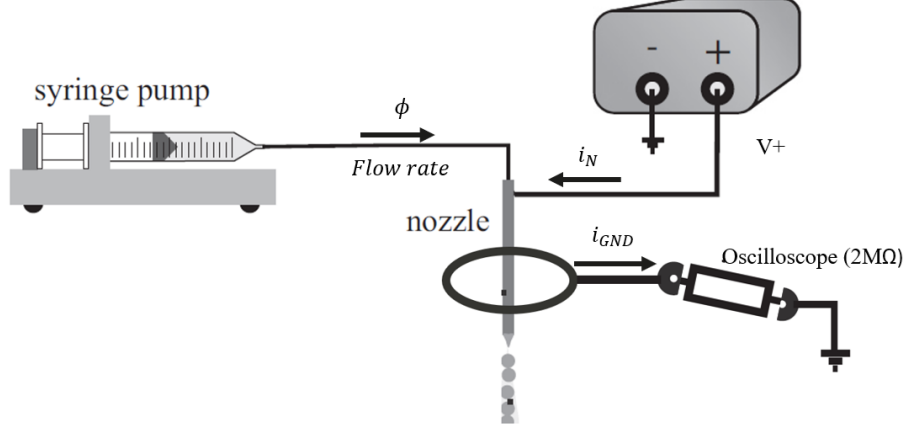

Figure 7. Setup used to reproduce Verdoold's classification method. Source: adapted from Verdoold et al. (2013).
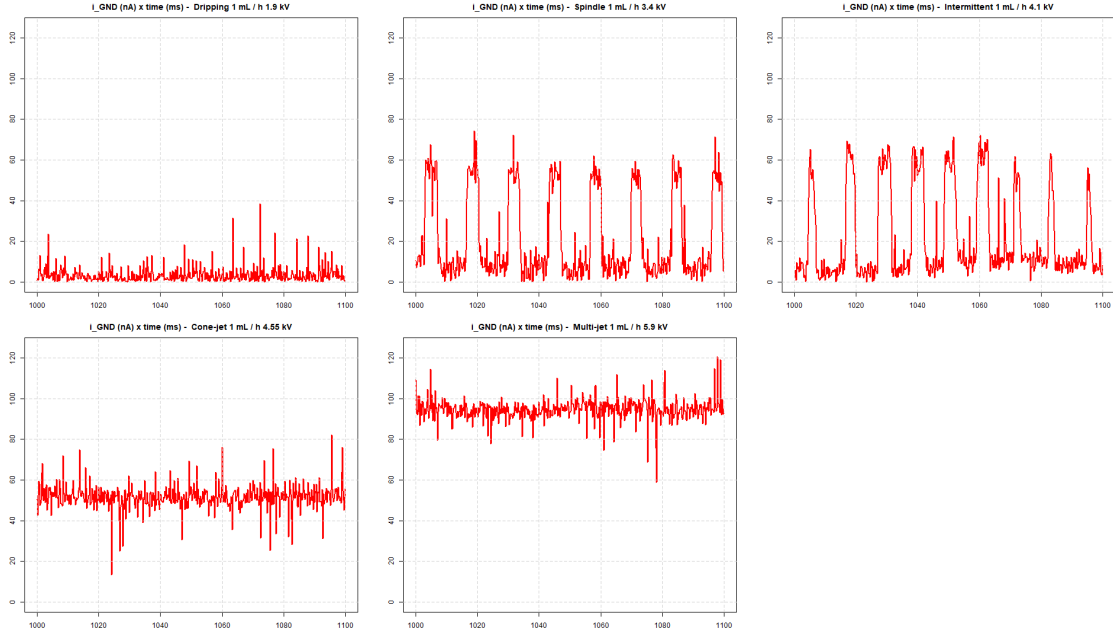
The results obtained are shown in Figure 8.

Figure 8. Results from the attempt to reproduce Verdoold's results on our setup.

As we can see in Figure 8, we see a clear distinction between the spray modes, which is what we wish to see in the multinozzle. We can conclude that our measurement methodology can reproduce the results, therefore it must be something in the multinozzle that is "hiding" the intermittent spray signal.

Comparing the single nozzle setup on Figure 7 and the multinozzle on Figure 3, the most significant difference is indeed the presence of the crown. Therefore, let's begin

7

by understanding the influence of the crown on i_{GND}, which is the current that we know is capable of showing a distinction of spraying modes.

3.3   Crown influences on i_{GND}

To understad the influence of the crown on the ground current, we'll use the same setup shown on Figure 3, but we'll make $V_+ = 0\,\text{V}$, $\phi = 0\,\text{mL/h}$ and measure i_{GND} for different crown voltages. Since there is no flow and no positive voltage, we'll be measuring the current on the groung ring introduced by the crown only. In addition, we'll use coaxial cables during the measurements.

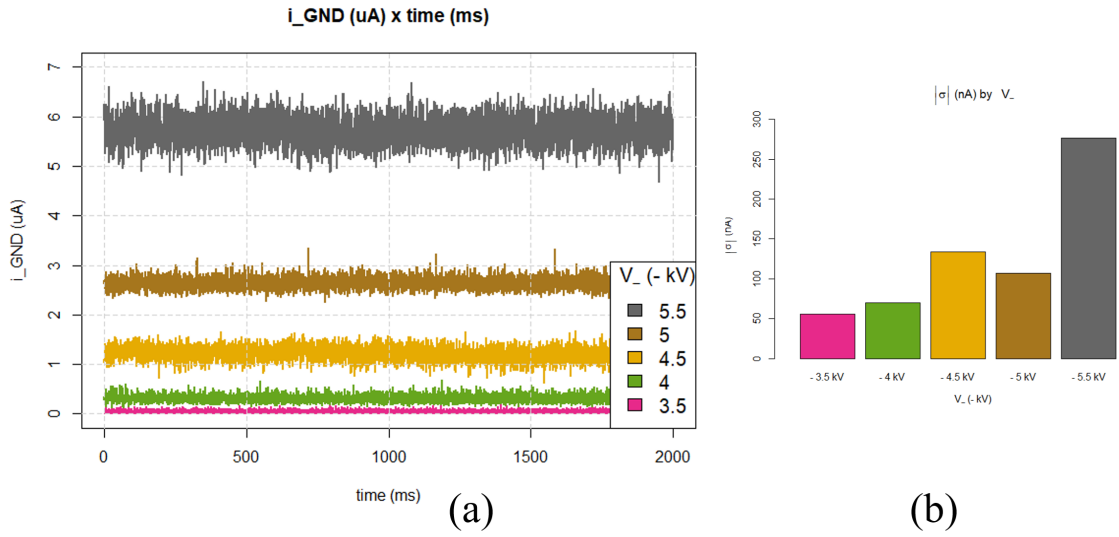Figure 9 shows the shape of i_{GND} for different values of V_-.

Figure 9. i_{GND} for different values of V_-. (a) Waveform and (b) standard deviation

As seen of Figure 9 (a), the crown alone introduces a signal on i_{GND} starting from $V_- = -4\,\text{kV}$, which increases in both average value and standard deviation as V_- increases. This is consistent with was happens at the crown: from $V_- = -4\,\text{kV}$ onwards the sharp needles of the crown begin to ionize the air, producing ions that can be directed to ground ring. This results in a current $i_{GND} > 0$ induced by the crown.

In addition, on Figure 9 (b) we see that the standard deviation introduced by the crown is significant. As we saw on Figure 8, the intermittent spray mode presents peaks in the current signal in order of 50 nA, but the "noise" introduced by the crown alone is already over 50 nA when $V_- = -4.5\,\text{kV}$, which is voltage used on the results of Figure 5. Therefore, it is reasonable to assume that the reason we are not seeing a good distinction between the spray modes on Figure 5 is because of this signal introduced by the crown alone.

3.3.1   Atenuating Crown Influences on i_{GND}

In order to verify the above hypothesis, we can try to reduce the influence of the crown in the signal and verify if the intermittent signal becomes distinguishable. We can achieve this adding digital filters in the oscilloscope software to remove the following frequencies:

- 50 Hz frequency from the electric grid: use a stop band in the range 48 - 52 Hz

- All frequencies above 100 Hz: use low pass filter with cut-off frequency 100 Hz.

Since the intermittent peaks are usually under 100 Hz (Verdoold et al., 2013), we can remove anything above this frequency from the signal as it is not what we wish to measure.

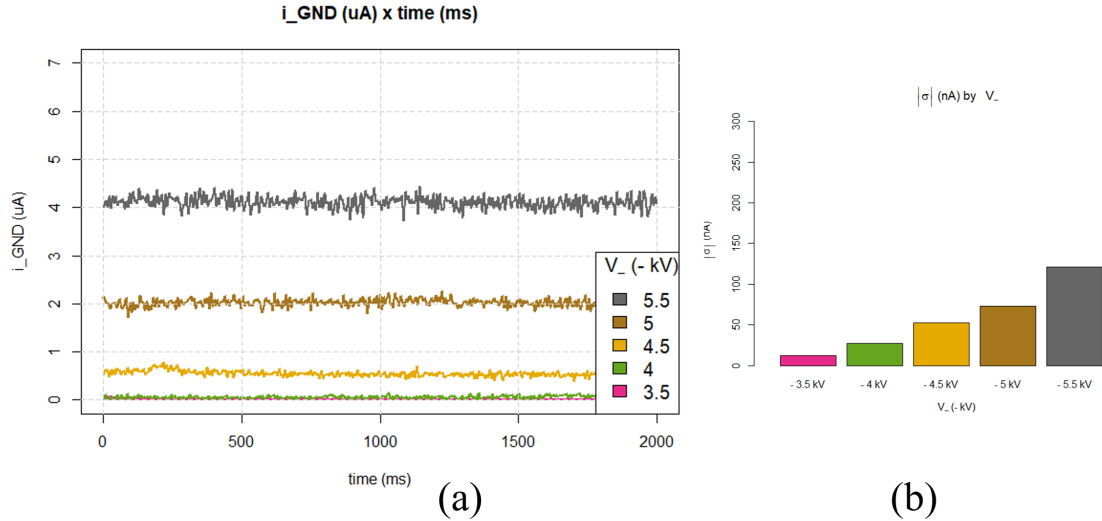Using this, we once again collect the signals of Figure 9, obtaining the signal on Figure 10.

Figure 10. i_{GND} for different values of V_- with digital filters. (a) Waveform and (b) standard deviation

Comparing Figure 10 and Figure 9, we see that the filters significantly reduce the standard deviation (i.e. the "noise") in i_{GND}. For $V_- = -4.5\,\text{kV}$, the standard deviation is already almost three times smaller. However, it remais above 50 nA, so it could still make it difficult to see the intermittent peaks in the signal. Ideally, we would use the $V_- = -4\,\text{kV}$ to get the smallest amount of noise introduced, but it is not clear if it possible to achieve a good neutralization with such a small V_-.

3.3.2   8 vs 16 Needles in the Crown

Around this time, Gilbert request us to test the crown with 8 needles for the WP2, as opposed to the 16 needles we had always used until this point. Difficulties to

9

reinsert removed needles meant that from this point onwards we would always use a needle with 8 needles.

Therefore, before we continue with this analysis, we need to understand how the signal introduces on i_{GND} has changed. We've re-done the test of Figure 10, obtaining the results shown on Figure 11
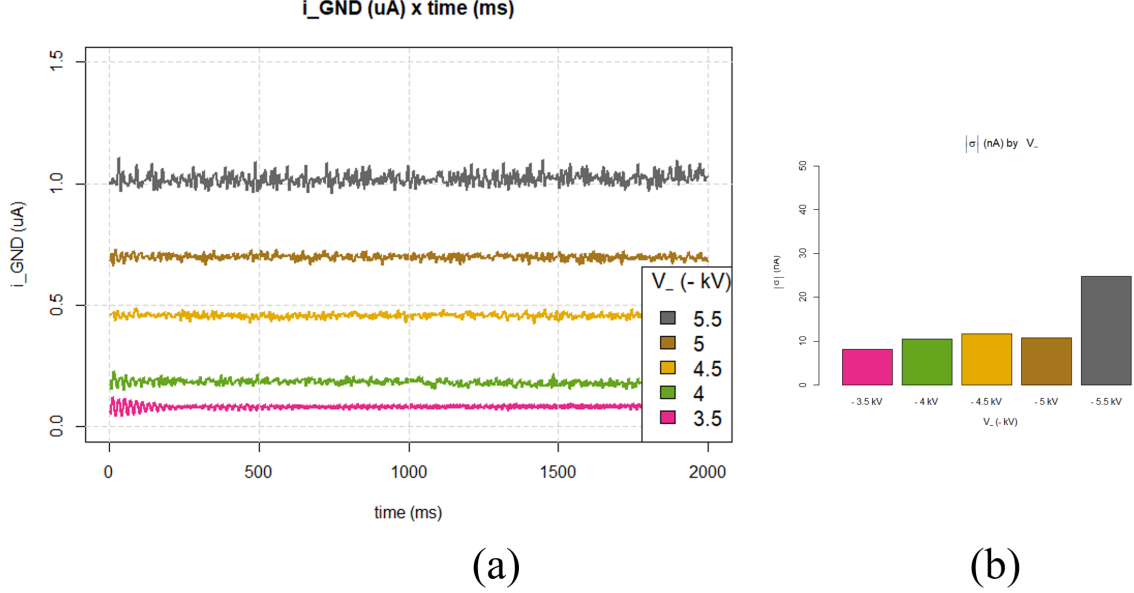

Figure 11. i_{GND} for different values of V_- with digital filters - Crown with 8 needles. (a) Waveform and (b) standard deviation

Comparing Figure 10 and Figure 11, we see that the 8 needles introduce a much smaller signal on the i_{GND}, both in terms of average value as in standard deviation. This will be helpful to make the intermittent peaks on the signal more visible, as for $V_- = -4.5\,\text{kV}$ the introduced standard deviation is only 10 nA.

3.4   Classifying the Spraying Mode

With everything that we've now learned about the influence of the crown and the necessity of filters, we can now repeat the experiment of Figure 3, using the same setup of Figure 3, but again only measuring i_{GND}. The oscilloscope was configured with $f_s = 5\,\text{kHz}$ and a sample size of $N_s = 20.000$. The crown had 8 needles and was fixed with $V_- = -4\,\text{kV}$ to reduce as far as possible the influence of the crown on i_{GND}.

Figure 12 shows the result obtained. The intermittent is clearly distinguishable from the cone-jet mode. However, expected, we cannot distinguish the elongated cone-jet and the multi-jet from the cone-jet.

Calculating the standard deviation on Figure 12 also allows for a good distinction between the spraying modes, as shown in Figure 13.

Based on Figure 13, we could use a simple if-else classification algorithm based on the standard deviation, defining a threshold for what is classified as intermittent or
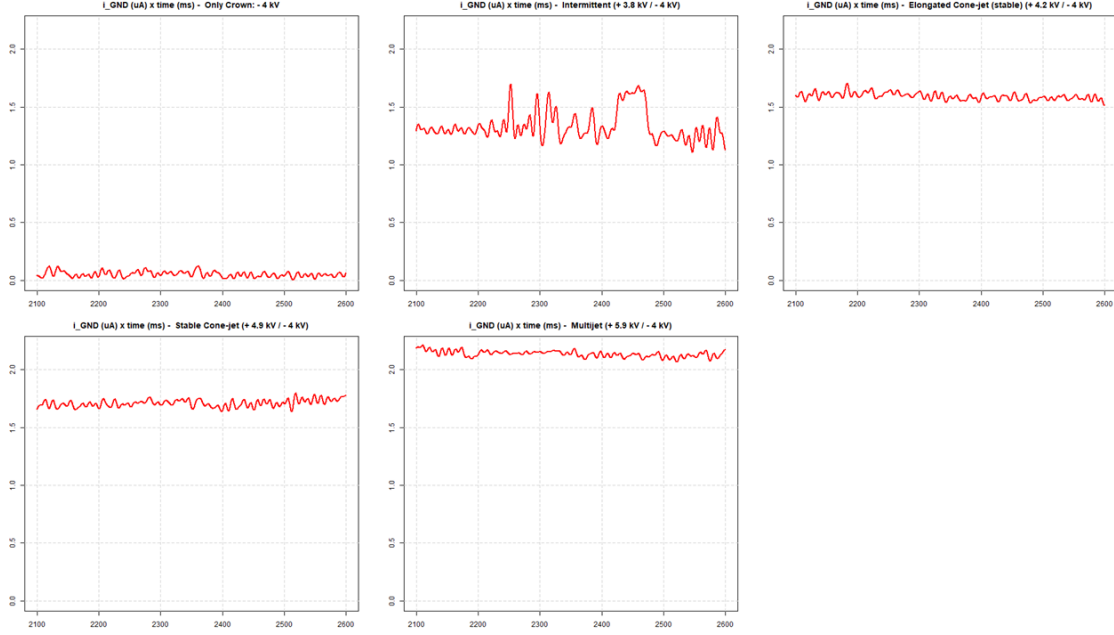
Figure 12. i_{GND} for different spray modes.
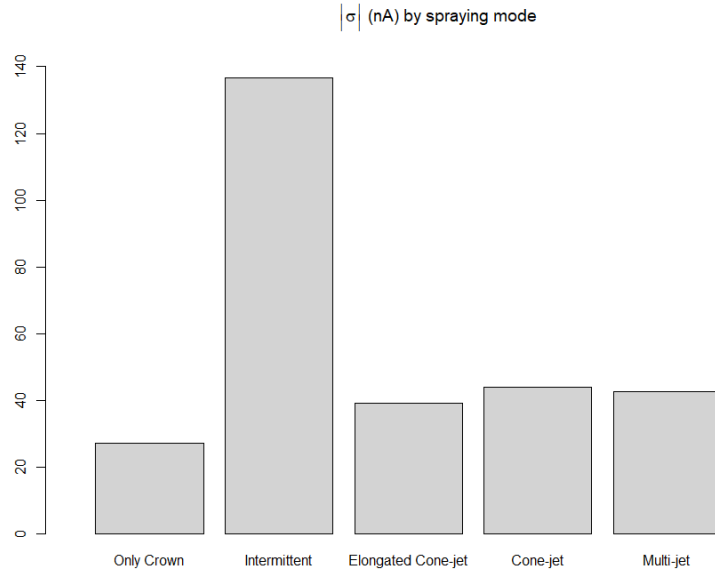
Figure 13. Standard deviation of i_{GND} for different spray modes.

cone-jet. For example, we could say that if $\sigma > 60\,\text{nA}$ then it is intermittent, else it is cone-jet (once inside the stable region defined by the mapping of the WP1). An algorithm for this will be further explored on subsection 3.7.

3.5   Optimizing the Signal Acquisition

In the previous sections, the signal was acquired using the minimum sampling frequency suggested by the Verdoold et al. (2013) of $f_s = 5\,\text{kHz}$. A sample size of

$N_s = 20.000$ was used to obtain a spectral resolution of 0.25 Hz for frequency domain anaysis, also suggested by Verdoold as the minimum. However, talks with Gilbert showed that the sampling frequency was too computationally expensive and the sample size was too slow, as it resulted in a sampling time window of 4 seconds, which is too large.

Therefore, to attempt to meet these requirements, we need to find the minimum sampling frequency and minimum sample size that can still reliably distinguish the signal of the intermittent from the cone-jet.

To do this, we'll use the following method:

- Collect a time window of $T = 100$ seconds for different values of f_s, resulting in a sample size of $N_s = T \cdot f_s$

- Break the $T = 100$ seconds into smaller time windows - denoted as S_i - of size T_S.

- Calculate the relevant statistical parameters in each S_i and store these values in an array of size T/T_S

- Plot a boxplot of the calculated statistical parameters

Figure 14 further explains the method above visually. T_S will be chosen for different values for the result to be verified. Note that $i = 1, 2, ..., T/T_S$, and the goal is to find the minimum T_S.
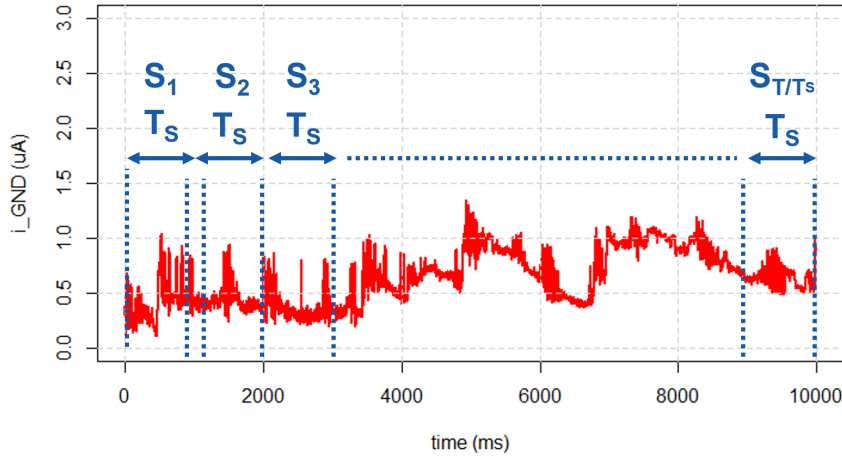

Figure 14. Method to find the minimum sample size that can still classify the EHDA mode via the current.

We'll use the same setup shown in Figure 3, using only the oscilloscope for i_{GND}. We begin with $f_s = 5\,\text{kHz}$, with $T_S = 0.01\,\text{s}; 0.1\,\text{s}; 1\,\text{s}; 10\,\text{s}$. Note that we are first changing T_S over four orders of magnitude to understand the general influence of T_S on the calcualated standard deviation. The result obtained is shown on Figure 15.

As we can see on Figure 15, $T_S = 1\,\text{s}$ appears to be the best sample size to differentiate between the intermittent and the cone-jet. Other orders of magnitude of
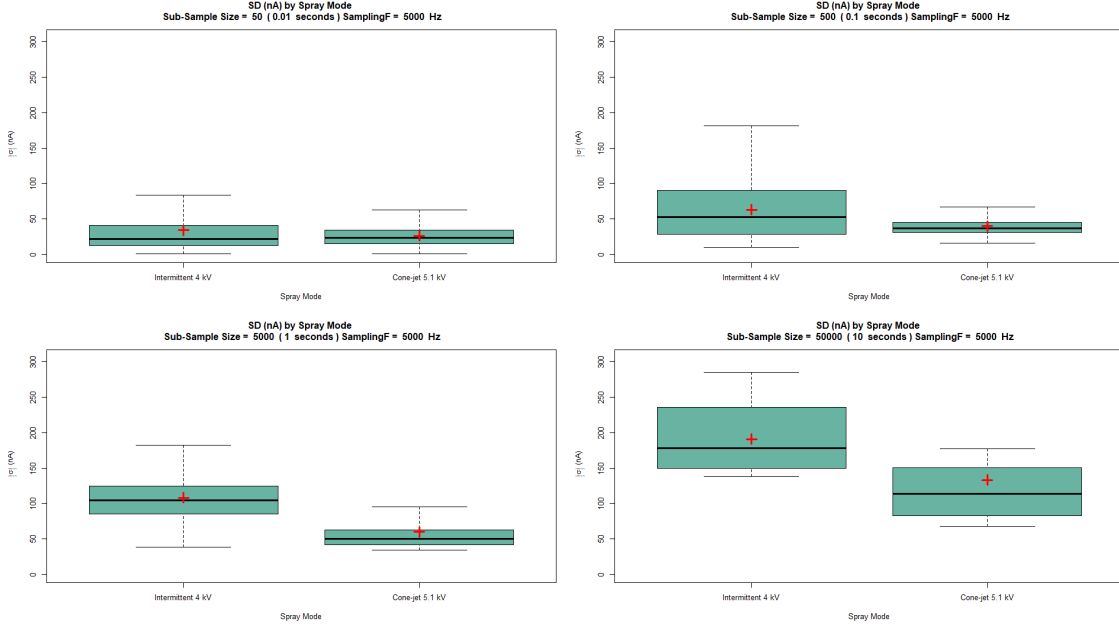
Figure 15. Calculated standard deviation for $f_s = 5\,\text{kHz}$, with $T_S = 0.01\,\text{s}; 0.1\,\text{s}; 1\,\text{s}; 10\,\text{s}$

T_S do not allow for a clear distinction between spraying mode via the statistical values. The next test is to change T_S around 1 second and compare them, using $T_S = 0.25\,\text{s}; 0.5\,\text{s}; 0.75\,\text{s}; 1\,\text{s}$. Figure 16 shows the results obtained for this test.

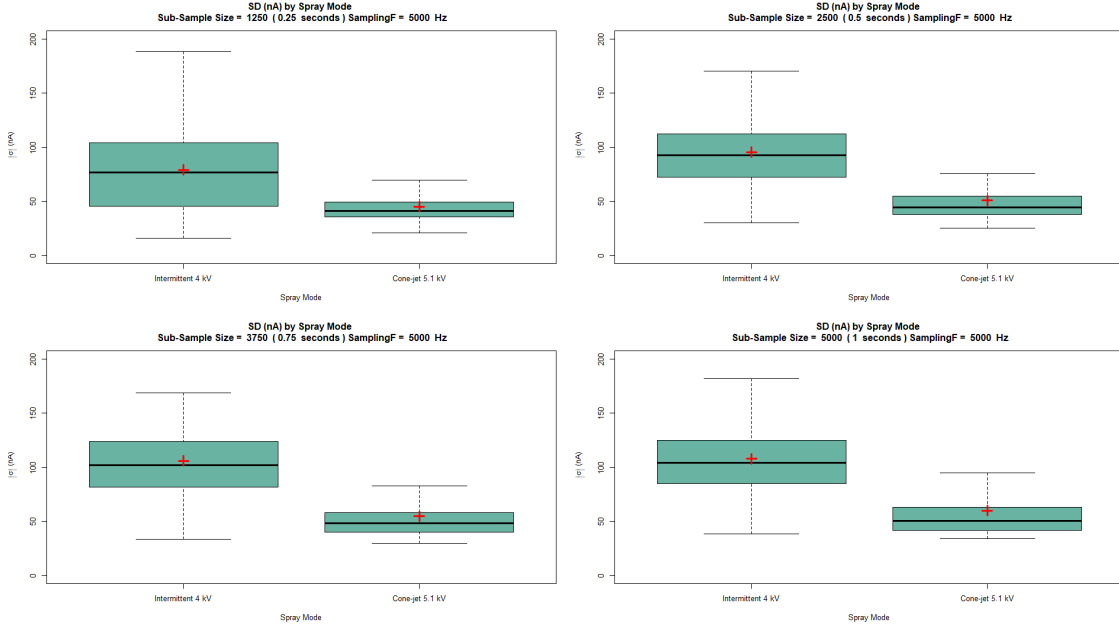**Figure 16.** Calculated standard deviation for $f_s = 5\,\text{kHz}$, with $T_S = 0.25\,\text{s}; 0.5\,\text{s}; 0.75\,\text{s}; 1\,\text{s}$

As seen on Figure 16, $T_S = 0.5\,\text{s}$ appears to be the smallest sample size that can differentiate the spraying modes. $T_S = 0.5\,\text{s}$ may still be feasible, but it presents significant overlapping between the two modes around $\sigma = 50\,\text{nA}$.

13

Now we need to find the minimum sampling frequency that can distinguish the spraying modes. We'll fix $T_S = 0.5\,\text{s}$ and compare the calculated statistical parameters for the following values of f_s: $f_s = 0.5\,\text{kHz}; 1\,\text{kHz}; 2\,\text{kHz}; 5\,\text{kHz}$. Figure 17 shows the result obtained for this test.
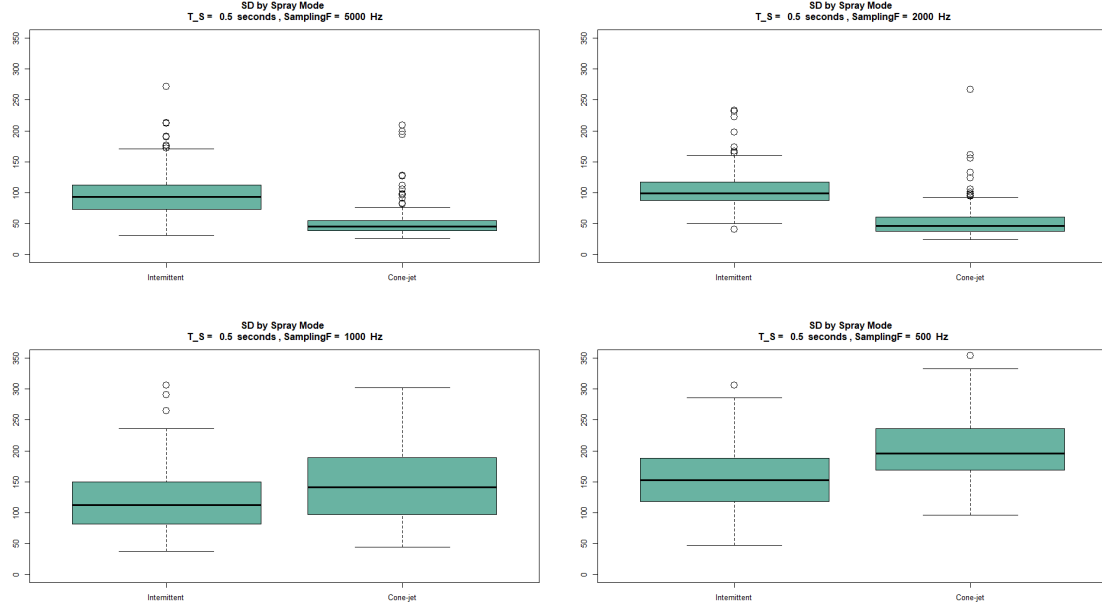
Figure 17.   Calculated standard deviation for $T_s = 0.5\,\text{s}$, with $f_s = 0.5\,\text{kHz}; 1\,\text{kHz}; 2\,\text{kHz}; 5\,\text{kHz}$

As we can see on Figure 17, $f_s = 2\,\text{kHz}$ appears to the be the smallest sampling frequency that can still distinguish the spraying modes.

The conclusion we can derive from these tests is that $T_S = 0.5\,\text{s}$ and $f_s = 2\,\text{kHz}$ are the mininum sample size and sampling frequency that can distinguish the spraying modes via statistical parameters. Note that this results in a sample size of $N_s = T_S f_s = 1.000$, which uses significantly less memory than the $N_s = 20.000$. We'll move forward with these values of N_s and f_s, seeking to test the classification with parameters that are consistent with Gilbert's requirements.

3.6   Optimizing the Classification

3.6.1   Trying different statistical parameters

So far, we've only the standard deviation of the signal to differentiate the spraying modes. However, we can also use other statistical parameters to distinguish the waveforms. The first one that we can try is the Relative Standard Deviation (RSD), defined on Equation 1

$$RSD = \left| \frac{\sigma}{\bar{\bar{I}}} \right| \tag{1}$$

where

- σ: standard deviation

- $\bar{I}$: arithmetic mean

Table 1 shows how the RSD can be a useful metric in the classification. When the spraying mode is intermittent, we expect the signal to display a large σ and a small $\bar{I}$, since the potential is lower and therefore also the mean value of the current in the system. This results in an overall value large value of the ratio.

Table 1. Expected behaviour of RSD for different spraying modes.

	Intermittent	Cone-jet
Numerator (σ)	HIGH	LOW
Denominator ($\bar{I}$)	LOW	HIGH
Overall Ratio ($\sigma/\bar{I}$)	LARGE	SMALL

On the other hand, when we have a cone-jet, we expect the signal to display a small σ - as the signal is much more stable - and a larger $\bar{I}$, given the larger potential. This results in an overall value small value of the ratio.

Therefore, both components of the fraction contribute in opposite directions to change the overall value of the ratio between the spraying modes, making this metric a potentially good classification parameter.

Figure 18 shows the the same result of Figure 17 using the RSD instead of the standard deviation.

As we can see on Figure 18, we can achieve a good distinction between the spraying modes with the RSD. However, the order of magnitude of the value is very small, which can be inconvenient. A simple to resolve this is take the inverse of the RSD, that we can define as the Signal-to-Noise Ratio (SNR), shown on Equation 2

$$SNR = \frac{1}{RSD} = \left| \frac{\bar{I}}{\sigma} \right| \tag{2}$$

In Equation 2, we call the standard deviation as the "noise", and the mean as the "signal". Figure 19 shows the same result of Figure 17 using the SNR.

As seen on Figure 19, the SNR is also a good metric to distinguish the intermittent and cone-jet modes. Unlike the RSD, the SNR spreads from the range 0 - 50, making it more convenient that the RSD and showing less outliers. Therefore, the RSD will be used from this point on, using $f_s = 2\,\text{kHz}$ and $N_s = 1.000 \quad (T_S = 0.5\,\text{s})$.
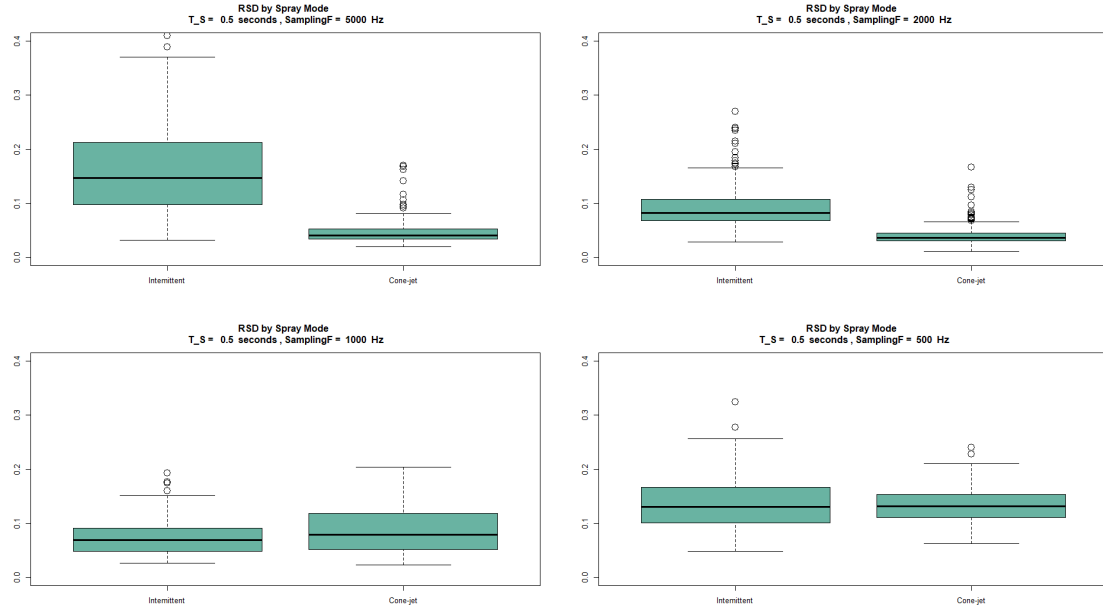
3.6.2 Classification via small Neural Networks

ASK BEN

15

Figure 18. Calculated RSD for $T_s = 0.5\,\text{s}$, with $f_s = 0.5\,\text{kHz};1\,\text{kHz};2\,\text{kHz};5\,\text{kHz}$
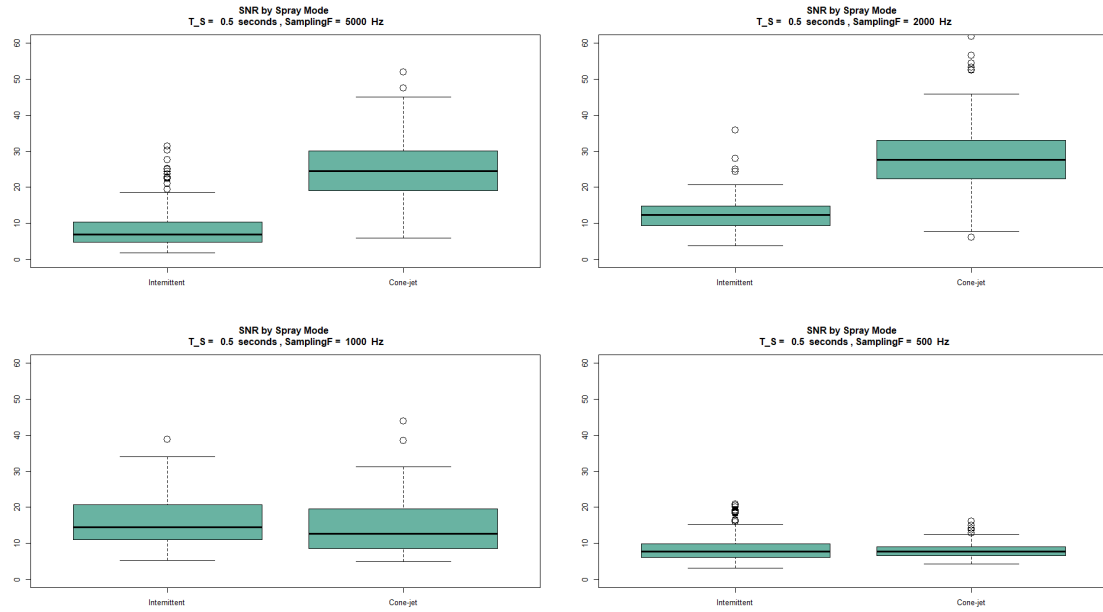
Figure 19. Calculated SNR for $T_s = 0.5\,\text{s}$, with $f_s = 0.5\,\text{kHz};1\,\text{kHz};2\,\text{kHz};5\,\text{kHz}$

3.7 Proof-of-Concept Real-time EHDA Classification

TODO

- try to reduce sample window
- use subsequent windows

- show commmon issues (step in the current value, etc)

- add pseudocode + complexity

3.8   Proof-of-Concept Real-Time EHDA Control

TODO

- problem wth subsequent window: how will it take into account the adjusts we're making:

- is it fast enough? if it even works at all!

- add pseudocode + complexity

4   Other Results

4.1   Relation between i_N, i_{GND} and i_C

During the experiments of Figure 4, where the three currents of the system were measured, we found a relation between the values of i_N, i_{GND} and i_C. It appeared that i_C was the sum of i_{GND} and i_N, in the direction defined at Figure 2. In this case, we'd find that

$$i_c = i_N + i_{GND} \tag{3}$$

In other to experimentally verify Equation 3, we defined two parameters:

$$DIFF = i_- - (i_{GND} + i_N) \tag{4}$$

$$DIFF = \frac{i_- - (i_{GND} + i_N)}{i_-} \cdot 100\% \tag{5}$$

Both parameters on Equations 4 and 5 measure how close Equation 3 is to zero, which should be case if Equation 3 is true. Calculating the value of theses parameters on the data of Figure 4 results in Table 2.

As we can see on Table 2, $i_N + i_{GND}$ is always within 5% of the absolute value of i_C, regardless of potential, flow rate or EHDA spray mode. We had discussions of whether or not this could be a useful metric for the control or the charge neutralization measurements, but we did not explore it further. We leave it here if it is something that Gilbert wishes to explore in the future.

Table 2. Calculated $DIFF$ parameters for the collected data of three currents

Condition	DIFF (nA)	DIFF (%)
Intermittent 20 mL / h	127,43	2,58
Intermittent 30 mL / h	107,66	1,74
Intermittent 50 mL / h	236,09	5,36
Cone-jet 20 mL / h	109,46	1,65
Cone-jet 30 mL / h	34,11	0,80
Cone-jet 50 mL / h	206,49	2,94
Multi-jet 20 mL / h	231,22	3,21
Multi-jet 30 mL / h	38,83	0,41
Multi-jet 50 mL / h	121,08	1,09

4.2 Inrush Current on i_N Measurements

During the work, Gilbert requested us to verify the spike of current on i_+ when switching on V_+. To do this, we used the same setup of Figure 3, only measuring the current i_+ with the oscilloscope. V_- was fixed on $V_- = -4.5\,\text{kV}$, with $\phi = 30\,\text{mL/h}$. The oscilloscope was configured for $f_s = 50\,\text{kHz}$ to capture the fast response of the inrush current. V_+ was switched on from $V_+ = 0$ to $V_+ = 5kV$, while V_- was already swicthed on. Figure 20 shows the result obtained in this test.

Figure 20 (a) shows that we have a short spike in the current, better viewed on Figure 20 (b). The initial spike lasts for about 6 ms and has a peak value of $i_+ = 4\,\text{uA}$. About 1 second after switching V_+ on, the current achieves it's peak overshoot value of $i_+ = 4.5\,\text{uA}$. 2.5 seconds after switching V_+ on the current stabilizes on its final value of $i_+ = 3\,\text{uA}$.

Both peaks of current Figure 20 (a) are about 50% higher than the final value of i_+, and well below the safety threshold of 10uA given by Gilbert. We did not see a large difference on i_+ when switching both V_+ and V_- on at the same time.

Notice that the FUG HV power supply accused a very large inrush current on its display, as shown on Figure 21. However, this value contradicts the value given by the oscilloscope, which is a better measurement instrument. In addition, if indeed we had $i_+ = 59\,\text{uA}$ as the FUG displays, it would have resulted in a voltage drop of $\Delta V = 118\,\text{V}$ accross the oscilloscope in series with V_+, which would have fried the channel according to instrument's datasheet. This was not the case, and therefore the physical evidence suggests that the inrush current in indeed as low as the oscilloscope suggests.
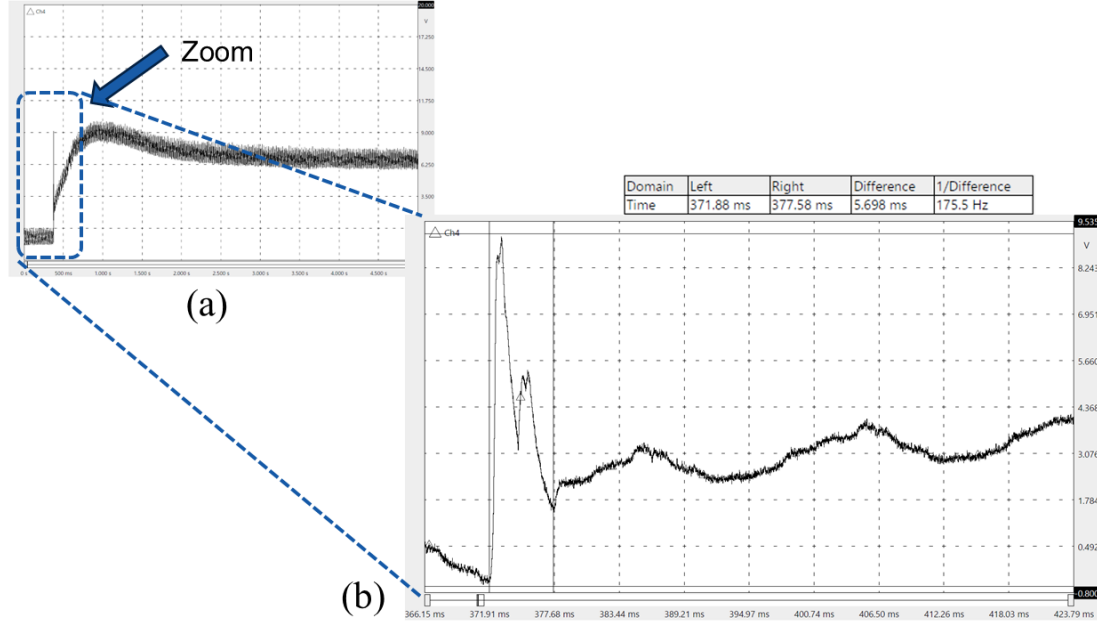
Figure 20. Inrush current measured on i_+ (a) over a 5 second time window and (b) with a zoom on the initial spike.

Figure 21. Inrush current displayed by the FUG HV power supply.

4.3 Switching i_+ ON and OFF in a 2-second interval

Gilbert also requested us to verify the behaviour of i_+ over several switches on V_+ in an interval of 2 seconds. We used the same setup described for Figure 20, obtaining the result shown on Figure 22.

As seen on Figure 22, the inrush current peak is higher for the first time i_+ is swicthed on. After the first time, it is about 50% smaller. The overshoot peak, however, increses as the system is switched on and off several times. We believe this
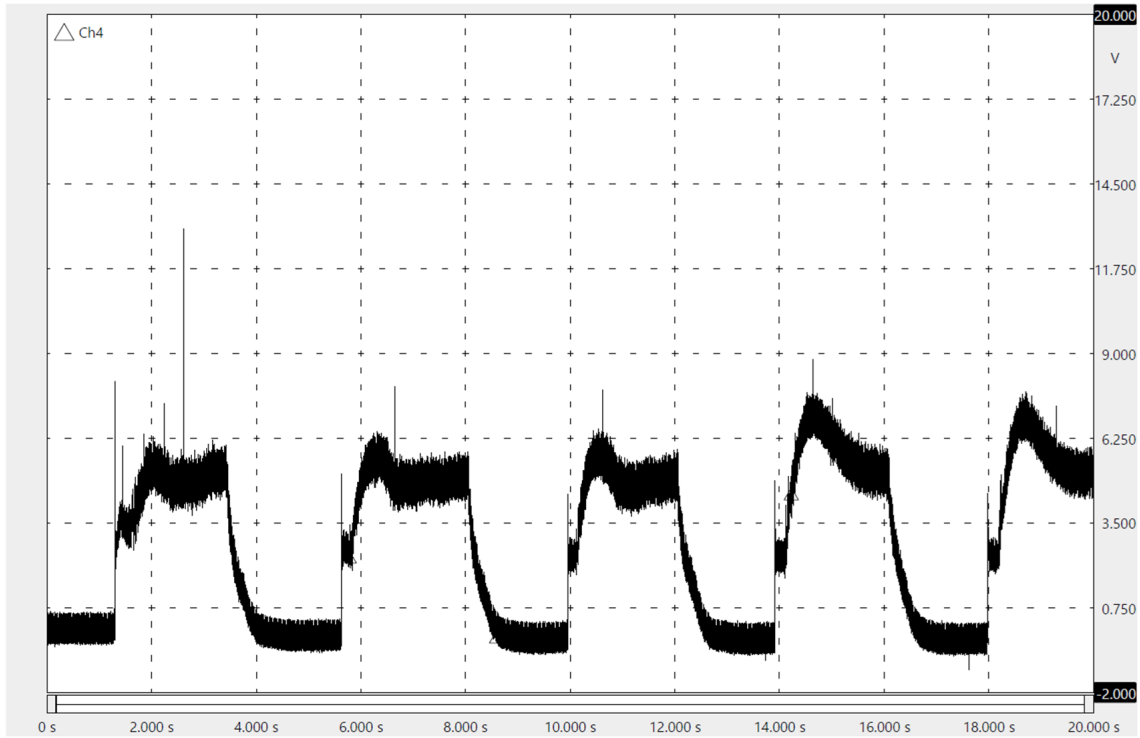
Figure 22.   Behaviour of i_+ when switching V_+ on and off in a 2-second interval.

is caused by the wetness that builds up on the nozzles.

References

Verdoold, S., Agostinho, L., Yutteri, C., and Marijnissen, J. (2013). A generic electrospray classification. *Journal of Aerosol Science*, 67:87–103.